Optics Letters

Generation of a frequency comb spanning more than 3.6 octaves from ultraviolet to mid infrared

Kana Iwakuni,[1,2] Sho Okubo,[2] Osamu Tadanaga,[3] Hajime Inaba,[2,*] Atsushi Onae,[2] Feng-Lei Hong,[2,4] and Hiroyuki Sasada[1]

[1]Department of Physics, Faculty of Science and Technology, Keio University, 3-14-1, Hiyoshi, Kohoku-ku, Yokohama, Kanagawa 223-8522, Japan
[2]National Metrology Institute of Japan (NMIJ), National Institute of Advanced Industrial Science and Technology (AIST), 1-1-1 Umezono, Tsukuba, Ibaraki 305-8563, Japan
[3]NTT Device Technology Laboratories, NTT Corporation, Atsugi shi, Kanagawa 243-0198, Japan
[4]Department of Physics, Graduate School of Engineering, Yokohama National University, 79-5 Tokiwadai, Hodogaya, Yokohama 240-8501, Japan
*Corresponding author: h.inaba@aist.go.jp

Received 14 July 2016; revised 3 August 2016; accepted 4 August 2016; posted 4 August 2016 (Doc. ID 270601); published 23 August 2016

We have observed an ultra-broadband frequency comb with a wavelength range of at least 0.35 to 4.4 μm in a ridge-waveguide-type periodically poled lithium niobate device. The PPLN waveguide is pumped by a 1.0–2.4 μm wide frequency comb with an average power of 120 mW generated using an erbium-based mode-locked fiber laser and a following highly nonlinear fiber. The coherence of the extended comb is confirmed in both the visible (around 633 nm) and the mid-infrared regions.

OCIS codes: (320.7090) Ultrafast lasers; (130.4310) Nonlinear; (300.6390) Spectroscopy, molecular; (120.3930) Metrological instrumentation.

http://dx.doi.org/10.1364/OL.41.003980

Optical frequency combs (OFCs) have been demonstrated to be powerful tools, not only for frequency metrology [1], but also for various applications, including laser sources in spectroscopy [2] and astrophysics [3]. In particular, OFCs with wide frequency coverages are desired for applications such as broadband dual-comb Fourier transform spectroscopy [4–7] and optical coherence tomography [8] because these OFCs can be used as light sources, and enable us to compare widely separated electromagnetic-wave frequencies in a direct manner. There are several approaches for generating a broadband OFC using nonlinear optical processes. For example, visible and/or near infrared broadband OFCs have been generated in a photonic crystal fiber (PCF) illuminated with an OFC based on several kinds of mode-locked lasers [1,9,10]. Similarly, near infrared broadband OFCs have been generated in a highly nonlinear fiber (HNLF) illuminated with an OFC based on a mode-locked laser [11–13]. Furthermore, mid-infrared broadband OFCs have been realized by difference frequency generation (DFG) using a waveguide-type periodically poled lithium niobate (WG-PPLN) device [14–16] or optical parametric oscillation [17]. A PCF usually requires a free-space optical coupling into the fiber with a narrow mode field, which is an obstacle to mechanical robustness and long-term operation. In contrast, HNLFs do not require a free-space optical coupling and have become mainstream in relation to broadband OFC generation. Therefore, broadband OFC generation using an HNLF is preferable in terms of practicality. Some visible broadband OFC generation without PCF or HLNF have been reported [18,19]. In particular, in [18], broadband visible combs are generated in a reverse-proton-exchange PPLN waveguide illuminated with a mode-locked fiber laser, which is promising for practical visible comb generation. In this Letter, we report on the generation of an ultraviolet-to-mid-infrared OFC using a WG-PPLN [15] and an HNLF. Specifically, we achieve ultraviolet OFC generation, and the maximum lower wavelength limit is 350 nm, which is the measurement limit of the optical spectrum analyzer. In addition, this method can be realized using an erbium-doped, fiber-based mode-locked laser with an output level of several tens of mW.

Figure 1 is a schematic diagram of the generation of an ultra-broadband comb. We used an Er-fiber-based mode-locked laser as described in [20] as the system light source. It emits a train of optical pulses at a wavelength of 1.56 μm with a repetition rate of 48 MHz and a power level of a few mW. The pulses are divided into four branches; one of them, which is used for wavelength conversion, is amplified to 120 mW with an

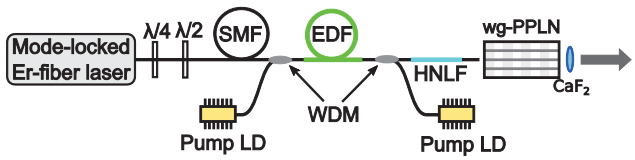

Fig. 1. Experimental setup for ultraviolet to mid-infrared comb generation. $\lambda/4$, quarter-wave plate; $\lambda/2$, half-wave plate; LD, laser diode; WDM, wavelength division multiplexing coupler; EDF, Er-doped fiber, HNLF, highly nonlinear fiber; WG-PPLN; waveguide-type periodically poled lithium niobate; CaF_2, calcium fluoride lens.

Er-doped fiber amplifier (EDFA) pumped both forward and backward by two 980 nm laser diodes. Subsequently, the amplified pulse train passes through a single-mode fiber (SMF) and is spectrally broadened from 1000 to 2400 nm in an approximately 15 cm long HNLF (wavelength dispersion; $+4.0\ \mathrm{ps \cdot nm^{-1} \cdot km^{-1}}$, nonlinear coefficient; $20\ \mathrm{W^{-1} \cdot km^{-1}}$). The output beam from the HNLF is then coupled into a WG-PPLN with a 28.55 μm period. The WG-PPLN was 24 mm long, 16 μm wide, and 12 μm high. The HNLF and the WG-PPLN are connected to another SMF about 15 cm in length. The polarization of the pulses on the WG-PPLN is adjusted to the desired linear state with a $\lambda/4$ and a $\lambda/2$ plate because the Er-fiber laser and the EDFA consist of non-polarization-maintaining fiber. The output pulses from the WG-PPLN are collimated by a CaF_2 lens and used for spectroscopy and frequency measurements, as described later. The operation is very stable because the system has an almost all-fiber configuration. In addition, the carrier-envelope offset (CEO) beat is detected in another branch and phase locked to an atomic clock.

Figure 2(a) shows the spectra of an ultra-broadband comb recorded with three optical spectrum analyzers, which cover the wavelength regions of 350 to 1700 nm (blue), 1200 to 2400 nm (green), and 2500 to 4500 nm (red). The vertical axis is in a logarithmic scale, and the noise floors of the individual analyzers are spectra without any optical input. The long and short wavelength limits of the comb are 4400 and 350 nm, respectively, which are determined by the spectral coverage of the analyzers. The recorded mid-infrared spectrum involves the absorption lines of carbon dioxide at 2.7 and 4.3 μm and the absorption band of water from 2.6 to 3.1 μm in the atmosphere. The noise floor is a measurement limit of the spectrum analyzers, and it is mainly limited by the readout noise of the analyzers. Figure 2(b) shows a spectrogram of a broadband comb dispersed with a grating and taken with a single-lens reflex digital camera, which clearly shows that the comb spectrum entirely covers the visible region. The spectral distribution is not uniform and can be varied by rotating the wave plates in Fig. 1. When the power level incident on the WG-PPLN is about 120 mW, the broadband comb provides about 30 mW for the visible region and about 250 μW for the mid-infrared region. In summary, the broadband comb extends across 3.6 octaves at its narrowest, which is the broadest OFC ever reported.

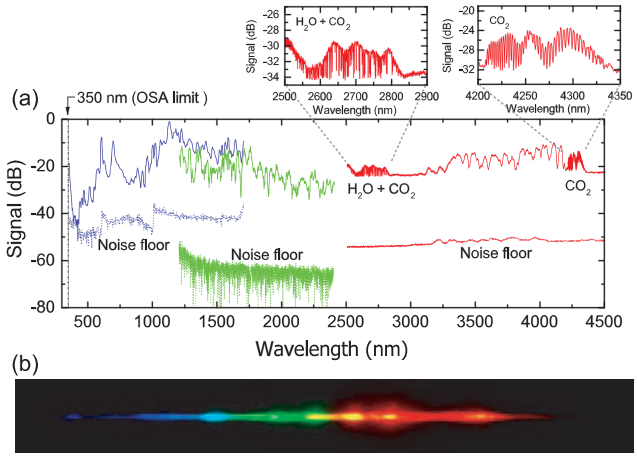

Fig. 2. (a) Observed broadband comb spectrum from 350 to 4500 nm and (b) a spectrogram of the broadband comb in the visible region.

Figure 3 depicts the RF spectrum of the comb in the mid-infrared regime observed with a liquid-nitrogen-cooled InSb photovoltaic detector. An optical bandpass filter limits the wavelength range of the comb to between 2.4 and 4.8 μm. A comb-like structure equally spaced at a repetition rate of 48 MHz is observed, which suggests that the comb in the mid-infrared regime has a high coherence. The amplitude of the beat notes decreases as the beat frequency increases because of the detector bandwidth of 100 MHz. In addition, the optical power per comb mode in the mid-infrared regime is approximately 200 pW when we assume a flat spectrum from 2500 to 4500 nm. This power level is sufficient for dual-comb spectroscopy. It may also be sufficient for beat counting if the power is enhanced at a desirable wavelength by changing the polarization state and the pump power.

Figure 4 shows the RF spectrum of the CEO beat in the red and green wavelength regions. We observed the CEO beat at around 30 MHz by detecting the comb component in the red or green wavelength region with a 125 MHz bandwidth Si photo detector. The detected 30 MHz signal is consistent with the stabilized CEO frequency at 30 MHz. Servo bumps resulting from the CEO frequency stabilization are also observed around (30 ± 0.5) MHz in Fig. 4(b). From the CEO beat detection, we consider two possible processes that generate the CEO beat:

(1) The ultra-broadband comb generation in the visible region is mainly due to the SHG and SFG of the infrared comb in the WG-PPLN ($\chi^{(2)}$ process). When some comb components are further generated based on the SFG of the visible comb and the infrared comb in the red and green wavelength regions, the CEO beat is detected based on the $2f$-$3f$ interference between the visible combs and the SFG combs in the red and green wavelength regions.

(2) The ultra-broadband comb generation in the visible region is mainly due to a $\chi^{(3)}$ process in the WG-PPLN (for example, the four-wave mixing process). When some comb

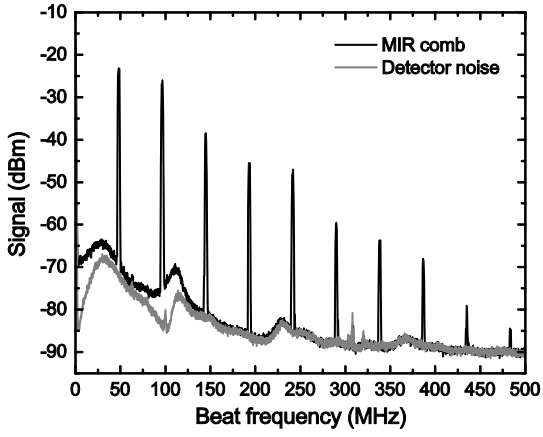

Fig. 3. RF spectrum of the mid-infrared part of the broadband comb shown in black and the detector noise (output from the detector without optical input) shown in gray. The RF spectrum analyzer was set at a resolution bandwidth of 1 MHz and a video bandwidth of 3 kHz.

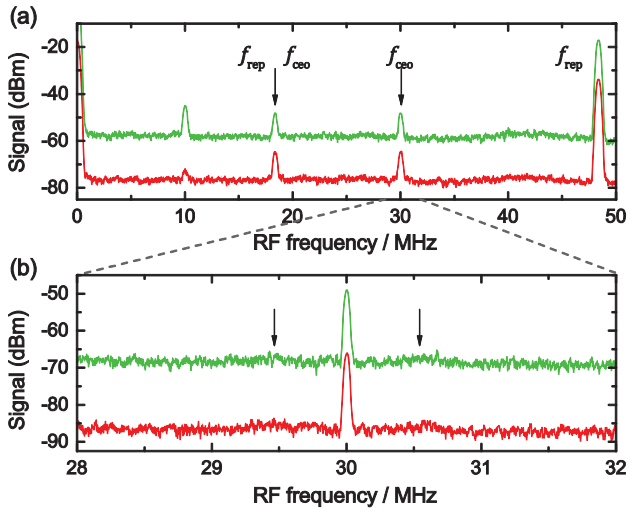

Fig. 4. (a) Carrier-envelope offset beats observed by detecting the comb components in the green and red wavelength regions. The upper and lower curves show the RF spectra observed in the green and red wavelength regions with an RBW of 300 kHz and a VBW of 3 kHz. The signals at 10 MHz are noise generated in an electric component between the photodetector and spectrum analyzer used for signal observation. (b) Magnified view of (a) around 30 MHz with an RBW of 30 kHz and a VBW of 300 Hz.

components are further generated based on the SHG of the infrared comb in the red and green wavelength regions, the CEO beat is detected based on the f-$2f$ interference between the visible combs and the SHG combs in the red and green wavelength regions.

Further investigations are needed to verify the possible processes for the ultra-broadband comb and CEO beat generation.

The broadband comb is used to measure the frequency of a 633 nm He–Ne laser. Figure 5(a) is a schematic diagram of the experimental setup. Beat notes between the comb modes and the He–Ne laser are detected with a Si avalanche photodiode. The detected signal is delivered to an RF spectrum analyzer and two independent tracking oscillators (TO #1 and TO #2). They are phase locked to the beat signal, and their frequencies are counted with two frequency counters. The output of TO #2 is also used to phase lock the beat signal at 30 MHz through the feedback to the offset-locked He–Ne laser [21]. Figure 5(b) presents the RF spectrum of beat notes between the He–Ne laser and the neighboring comb modes. The signal-to-noise ratio is approximately 20 dB at a resolution bandwidth of 300 kHz. Figures 5(c) and 5(d) show the temporal variation of the beat frequency of TO #1 and the frequency difference between TO #1 and #2 measured by the frequency counters with an averaging time of 1 s. The counted frequencies are consistent with each other for a duration exceeding 1000 s, which strongly suggests that the visible component generated by the method is available for frequency metrology. Although the result is not a proof, it is a prerequisite that there is neither cycle slips in the TOs nor count misses in the frequency counters during this period.

The mid-infrared part of the broadband comb is provided by DFG, in which the ordinary phase-matching conditions are satisfied. Figure 6 shows calculated signal and pump wavelengths that satisfy the phase-matching condition for generating

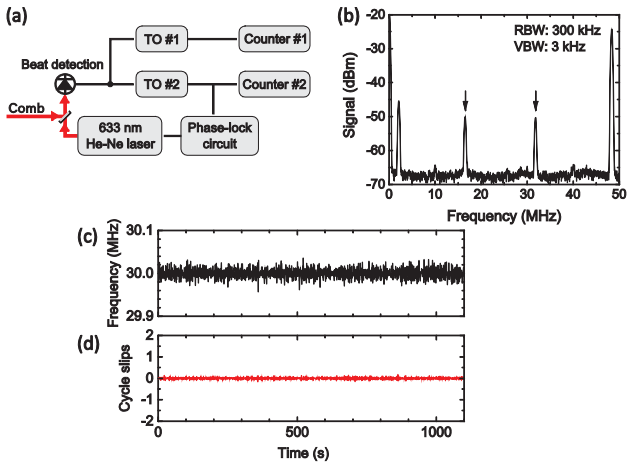

Fig. 5. (a) Experimental setup for the frequency measurement of a He–Ne laser. (b) RF spectrum of the beat notes. (c) Temporal variation of the beat frequency measured with counter #1. (d) Temporal variation of the frequency difference between counters #1 and #2.

the idler wavelength using the present WG-PPLN at room temperature (22.5°C). The upper and lower curves show the signal and pump wavelengths, respectively. The combination of signal and pump waves generates an idler wave that corresponds to the frequency difference shown on the horizontal axis. For example, a 1.7 μm signal wave and a 1.0 μm pump wave generate a 2.5 μm idler wave. Since the incident OFC spectrum (signal and pump waves) is broadened from 1.0 to 2.4 μm, according to Fig. 6, the output OFC (idler wave) can be generated from 2.5 to 4.5 μm, which is consistent with the results shown in Fig. 2(a). We also attempt to use WG-PPLNs with other lengths to generate an ultra-broadband comb. The output spectral broadening when using 12 and 36 mm long WG-PPLNs is much weaker and narrower than that of the 24 mm long WG-PPLN.

On the other hand, we have not yet completely understood how the ultraviolet and visible parts of the broadband comb are generated. To investigate this mechanism, we illuminate the WG-PPLN with the amplified Er-fiber comb without using the HNLF. The input comb is spectrally broadened at the

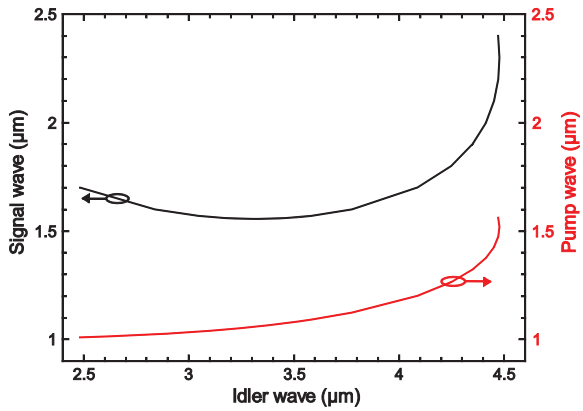

Fig. 6. Calculated signal and pump wavelengths required for generating the idler wavelength under the phase-matching condition when using a PPLN with 28.55 μm period at 22.5°C.

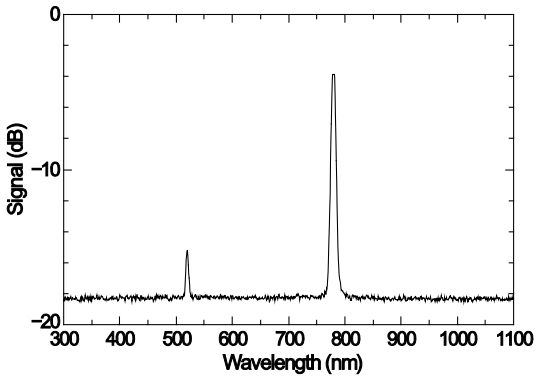

Fig. 7. Observed visible spectrum from the WG-PPLN illuminated with a 100 nm wide Er-fiber comb.

center (1550 nm), and its spectral bandwidth is about 100 nm, which is considerably narrower than that attained using the HNLF. Figure 7 shows the observed visible spectrum of the output from the WG-PPLN. It only contains the second (780 nm) and the third (520 nm) harmonics of the mode-locked laser (1560 nm), which matches the harmonic generation condition of the WG-PPLN. The result shows that it is essential that the comb incident on the WG-PPLN is greatly broadened for the ultra-broadband comb generation. This result also suggests that the ultra-broadband comb generation in the WG-PPLN is due to a $\chi^{(2)}$ process rather than a $\chi^{(3)}$ process.

In conclusion, we have developed a broadband optical frequency comb across more than 3.6 octaves from the ultraviolet to mid-infrared region using a WG-PPLN device. We observed that the mid-infrared component contributes to the absorption spectroscopy of water and carbon dioxide as a source. We demonstrated frequency measurements of a beat note between the comb and a 633 nm He–Ne laser. Furthermore, we undertook some additional experiments to understand ultra-broadband comb generation in the visible regime. We have already observed ultra-broadband comb generation almost continuously for more than six months without replacing the PPLN or HNLF. In addition, this method is universal because we observed very similar spectra using another laser system and another WG-PPLN chip. This shows that the repeatability and reproducibility of the method are good. Ultra-broadband comb generation will be widely used for various applications such as spectroscopy, astrophysics, and frequency metrology because of its simplicity and practicality.

Funding. Japan Society for the Promotion of Science (JSPS), Kakenhi (23244084); Ministry of Education, Culture, Sports, Science, and Technology (MEXT), Advanced Photon Science Alliance.

REFERENCES

1. S. A. Diddams, D. J. Jones, J. Ye, S. T. Cundiff, J. L. Hall, J. K. Ranka, R. S. Windeler, R. Holzwarth, T. Udem, and T. W. Hänsch, Phys. Rev. Lett. **84**, 5102 (2000).
2. F. Keilmann, C. Gohle, and R. Holzwarth, Opt. Lett. **29**, 1542 (2004).
3. T. Steinmetz, T. Wilken, C. Araujo-Hauck, R. Holzwarth, T. W. Hänsch, L. Oasquini, A. Manescau, S. D'Odorico, M. T. Murphy, T. Kentischer, W. Schmidt, and T. Udem, Science **321**, 1335 (2008).
4. I. Coddington, W. C. Swann, and N. R. Newbury, Phys. Rev. Lett. **100**, 013902 (2008).
5. T. Ideguchi, A. Poisson, G. Guelachvili, N. Picqué, and T. W. Hänsch, Nat. Commun. **5**, 1 (2014).
6. S. Okubo, K. Iwakuni, H. Inaba, K. Hosaka, A. Onae, H. Sasada, and F.-L. Hong, Appl. Phys. Express **8**, 082402 (2015).
7. F. C. Cruz, D. L. Maser, T. Johnson, G. Ycas, A. Klose, F. R. Giorgetta, I. Coddington, and S. A. Diddams, Opt. Express **23**, 26814 (2015).
8. T. Bajraszewski, M. Wojtkowski, M. Szkulmowski, A. Szkulmowska, R. Huber, and A. Kowalczyk, Opt. Express **16**, 4163 (2008).
9. C. Farrell, K. A. Serrels, T. R. Lundquist, P. Vedagarbha, and D. T. Reid, Opt. Lett. **37**, 1778 (2012).
10. N. Nishizawa, H. Mitsuzawa, J. Takayanagi, and K. Sumimura, J. Opt. Soc. Am. B **26**, 426 (2009).
11. T. Okuno, M. Onishi, T. Kashiwada, S. Ishikawa, and M. Nishimura, IEEE J. Sel. Top. Quantum Electron. **5**, 1385 (1999).
12. F. Tauser, A. Leitenstorfer, and W. Zinth, Opt. Express **11**, 594 (2003).
13. T. R. Schibli, K. Minoshima, F.-L. Hong, H. Inaba, A. Onae, H. Matsumoto, I. Hartl, and M. E. Fermann, Opt. Lett. **29**, 2467 (2004).
14. M. H. Chou, J. Hauden, M. A. Arbore, and M. M. Fejer, Opt. Lett. **23**, 1004 (1998).
15. O. Tadanaga, T. Yanagawa, Y. Nishida, H. Miyazawa, K. Magari, M. Asobe, and H. Suzuki, Appl. Phys. Lett. **88**, 061101 (2006).
16. C. Erny, K. Moutzouris, J. Biegert, D. Kühlke, F. Adler, A. Leitenstorfer, and U. Keller, Opt. Lett. **32**, 1138 (2007).
17. F. Adler, K. C. Cossel, M. J. Thorpe, I. Hartl, M. E. Fermann, and J. Ye, Opt. Lett. **34**, 1330 (2009).
18. C. Langrock, M. M. Fejer, I. Hartl, and M. E. Fermann, Opt. Lett. **32**, 2478 (2007).
19. T. M. Fortier, A. Bartels, and S. A. Diddams, Opt. Lett. **31**, 1011 (2006).
20. Y. Nakajima, H. Inaba, K. Hosaka, K. Minoshima, A. Onae, M. Yasuda, T. Kohno, S. Kawato, T. Kobayashi, T. Katsuyama, and F.-L. Hong, Opt. Express **18**, 1667 (2010).
21. J. Ishikawa, Appl. Opt. **34**, 6095 (1995).